ISSN 1070-3632, Russian Journal of General Chemistry, 2018, Vol. 88, No. 8, pp. 1681–1689. © Pleiades Publishing, Ltd., 2018.
Original Russian Text © E.V. Korneeva, O.V. Loseva, A.I. Smolentsev, A.V. Ivanov, 2018, published in Zhurnal Obshchei Khimii, 2018, Vol. 88, No. 8, pp. 1361–1370.

Reactivity of Silver(I) Diethyldithiocarbamate and Ion-Polymeric Complexes $\{[Au(S_2CNEt_2)_2][AgCl_2]\}_n$ and $\{[Au(S_2CNEt_2)_2]_2[AgCl_2]Cl\cdot 2H_2O\}_n$: Synthesis, Supramolecular Structures, and Thermal Behavior

E. V. Korneeva[a], O. V. Loseva[a], A. I. Smolentsev[b,c], and A. V. Ivanov[a]*

[a] *Institute of Geology and Nature Management, Far East Branch, Russian Academy of Sciences, per. Relochnyi 1, Blagoveshchensk, 675000 Russia*
**e-mail: alexander.v.ivanov@chemist.com*

[b] *Nikolaev Institute of Inorganic Chemistry, Siberian Branch, Russian Academy of Sciences, pr. Akademika Lavrent'eva 3, Novosibirsk, 630090 Russia*

[c] *Novosibirsk State University, ul. Pirogova 1, Novosibirsk, 630090 Russia*

Received March 28, 2018

Abstract—New ion polymeric gold(III)–silver(I) complexes, $([Au\{S_2CNEt_2\}_2][AgCl_2])_n$ and $([Au\{S_2CNEt_2\}_2]_2[AgCl_2]Cl\cdot 2H_2O)_n$ have been synthesized and characterized by X-ray diffraction data and IR spectra. The structure of the first complex is represented by $[Au\{S_2CNEt_2\}_2]^+$ complex cations and polymeric silver chloride anion $([AgCl_2]^-)_n$; the second complex consists of isomeric cations, linear $[AgCl_2]^-$ anions, chloride ions, and water molecules. Gold cations are involved in zigzag (AuAuAu angle 99.06°) and linear polymeric chains via secondary Au···S bond pairs. Thermal decomposition of the complexes with regeneration of gold and silver has been studied by simultaneous thermal analysis (STA).

Keywords: Silver(I) dithiocarbamates, ligand exchange, gold(III)–silver(I) complexes, ion polymeric complexes, supramolecular self-organization

DOI: 10.1134/S1070363218080200

Silver(I) thio- and dithiocarbamates exhibit considerable structural diversity, including monomeric, dimeric, hexameric, and polymeric compounds [1–7]. Heteroleptic silver(I) complexes with dithiocarbamate ligands can be regarded as molecular precursors of acanthite (α-Ag_2S) films [8–10] that are promising for the design of ion-selective electrode membranes and photoelectrochemical cells for solar hydrogen generation by decomposition of water. Many silver(I) compounds have low toxicity and exhibit high antitumor, antibacterial, and anti-inflammatory activities and are sources of biologically active silver ions with prolonged action [11–14].

Gold(III) dithiocarbamato-chlorido (-bromido) complexes and gold(I) heteroleptic complexes also act as efficient anticancer agents [15–18]. (The complex $[Au\{S_2CN(CH_2)_5\}Cl_2]$ has been reported by us [19] simultaneously with Zhang et al. [18]). It seemed important to obtain new dithiocarbamato-chlorido complexes containing both gold(III) and silver(I) at different ratios.

We previously found high efficiency of $AuCl_3$ binding from acidic (2 M HCl) solutions by a number of transition and post-transition metal dithiocarbamates with the formation of Au(III) [19, 20] and Au(III)–Au(I) [21] dithiocarbamato-chlorido complexes and double compounds with intricate supramolecular structures, which contained Bi(III) [22], Fe(III) [23], Zn(II) [24], Cd(II) [25], Hg(II) [26], and Tl(III) [27] in addition to Au(III). In continuation of these studies, we examined the ability of freshly prepared silver(I) diethyldithiocarbamate to bind gold(III) from saturated solutions of NaCl. As a result, we isolated new ion–polymer gold(III)–silver(I) dithiocarbamato-chlorido complexes with Au–Ag ratios of 1 : 1 (**1**) and 2 : 1 (**2**) and characterized them by X-ray diffraction, IR spectroscopy, and simultaneous thermal analysis data.

Table 1. Crystallographic data, experimental parameters, and structure refinement parameters for complexes **1** and **2**

Parameter	**1**	**2**
Formula	$C_{10}H_{20}N_2S_4Cl_2AuAg$	$C_{20}H_{44}N_4O_2S_8Cl_3Au_2Ag$
M	672.26	1237.22
Crystal system	Triclinic	Monoclinic
Space group	P-1	$P2/c$
a, Å	7.5243(9)	13.1045(8)
b, Å	8.9966(12)	8.1385(4)
c, Å	14.159(2)	18.5891(12)
α, deg	91.192(5)	
β, deg	93.615(4)	90.002(2)
γ, deg	91.938(4)	
V, Å^3	955.8(2)	1982.5(2)
Z	2	2
d_{calc}, g/cm^3	2.336	2.073
μ, mm^{-1}	9.398	8.519
F(000)	636	1184
Crystal dimensions, mm	0.28×0.14×0.02	0.25×0.22×0.20
Data collection range θ, deg	2.27–27.68	2.19–27.50
Reflection indices	$-9 \le h \le 9$, $-11 \le k \le 11$, $-2 \le l \le 18$	$-9 \le h \le 17$, $-5 \le k \le 10$, $-24 \le l \le 22$
Total number of reflections	9204	6826
Number of independent reflections	4317 (R_{int} = 0.0351)	4430 (R_{int} = 0.0280)
Number of reflections with $I > 2\sigma(I)$	3921	2668
Number of variables	186	195
Goodness of fit	1.064	0.853
Divergence factors [reflections with $F^2 > 2\sigma(F^2)$]	R_1 = 0.0613, wR_2 = 0.1913	R_1 = 0.0308, wR_2 = 0.0567
Divergence factors (all independent reflections)	R_1 = 0.0662, wR_2 = 0.1947	R_1 = 0.0640, wR_2 = 0.0629
Residual electron density (min/max), e/Å^3	–3.277/3.950	–0.803/0.817

The formation of complexes **1** and **2** can be represented by Eq. (1) which implies complete ligand redistribution between gold(III) and silver(I) coordination spheres:

$$6[Ag\{S_2CNEt_2\}] + 3Na[AuCl_4] + NaCl = \underset{\mathbf{1}}{[Au\{S_2CNEt_2\}_2][AgCl_2]} + \underset{\mathbf{2}}{[Au\{S_2CNEt_2\}_2]_2[AgCl_2]Cl} + 4Na[AgCl_2]. \quad (1)$$

Analogous behavior of silver(I) diethyldithiocarbamate, involving ligand exchange, was observed previously in the reactions with nickel(II) and platinum(II) complexes [28].

The IR spectra of crystalline compounds **1** and **2** contained intense absorption bands at 1566 (**1**) and 1548 cm^{-1} (**2**) due to stretching vibrations of C–N bonds in the dithiocarbamate groups =NC(S)S– [29, 30]. In both cases, the ν(C–N) frequency is intermediate between those typical of single C–N (1250–1360 cm^{-1}) and double C=N bonds (1640–1690 cm^{-1}), and the bands are considerably shifted toward higher frequencies, indicating partially double character of the N–C(S)S bond [30–32]. It follows from the given data that the N–C(S)S bond in complex

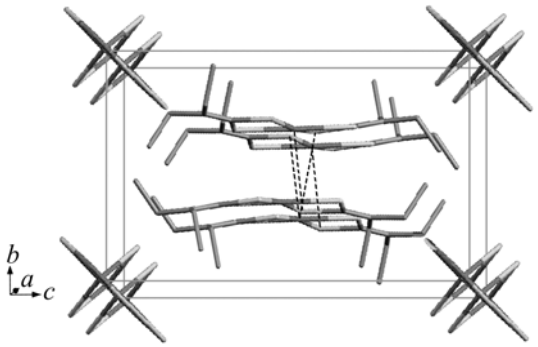

Fig. 1. Unit cell of complex **1** in crystal.

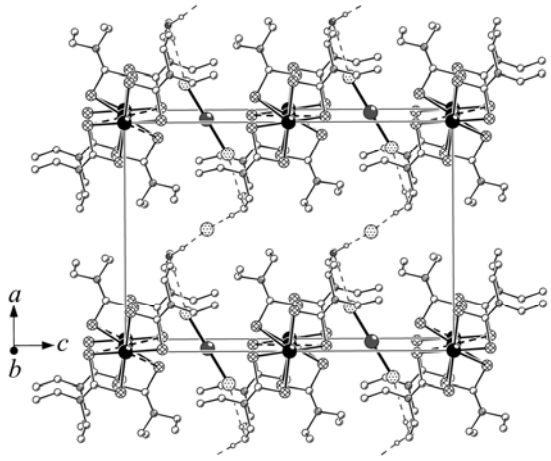

Fig. 2. Unit cell packing of complex **2** in crystal; projection onto the *ac* plane.

1 is shorter than in **2**. Unlike complexes **1** and **2**, silver(I) diethyldithiocarbamate displays a lower stretching frequency (1482 cm^{-1}) of the thioureide group.

Medium-intensity bands at 1155 (**1**) and 1154 cm^{-1} (**2**) and 989 (**1**) and 990 cm^{-1} (**2**) were assigned to antisymmetric (ν_{as}) and symmetric (ν_s) C(S)S stretching vibrations [29, 30, 33]. A weak band at 560 cm^{-1} (**1**, **2**) arises from ν(C–S) [34]. The region 2867–2982 cm^{-1} contains absorption bands due to C–H stretching vibrations of alkyl groups in the ligands. The IR spectrum of **2** characteristically showed an absorption band at 3550–3200 cm^{-1}, which is typical for crystallization water [35]; no such band was observed in the spectrum of **1**.

The unit cells of complexes **1** and **2** consist of two $[Au(S_2CNEt_2)_2][AgCl_2]$ or $[Au(S_2CNEt_2)_2]_2\cdot[AgCl_2]Cl\cdot 2H_2O$ units (Table 1; Figs. 1, 2). The structural units of both compounds are complex $[Au(S_2CNEt_2)_2]^+$ cations and $[AgCl_2]^-$ anions. Complex **1** contains a structurally unique non-centrosymmetric gold(III) cation (Fig. 3a), whereas two isomeric centrosymmetric cations, **A** (Au^1) and **B** (Au^2) were found in the crystal structure of complex **2** (Figs. 4a, 4b).

There are two diethyldithiocarbamate ligands in each cation; the ligand coordination is close to *S*,*S*′-isobidentate: the Au–S bond length ranges from 2.322 to 2.347 Å, which is typical for gold(III) complexes with dithiocarbamate ligands [25–27, 36]. This coordination mode implies formation of two small-sized four-membered metallacycles $[AuS_2C]$ having a common gold atom, which means the formation of the bicyclic fragment $[CS_2AuS_2C]$. The interatomic distances Au–C 2.855, 2.857 (**1**) and 2.818, 2.826 Å (**2**) in the rings are considerably smaller than the sum of the van der Waals radii of the gold and the carbon atoms (3.36 Å [37]), indicating transannular interactions between them. Judging by the torsion angles AuSSC and SAuCS (Table 2), mutual arrangement of atoms in the cyclic fragments $[AuS_2C]$, does not deviate from coplanarity to an appreciable extent. The square-planar structure of the $[AuS_4]$ chromophore suggests low-spin dsp^2-hybrid state of the gold atom.

The C_2NCS_2 fragments of the diethyldithiocar-bamate ligands are almost planar (see the torsion angles CNCS in Table 2); appreciable deviations from planarity were observed only for the C^6 atom of **1** and C^1 atom of cation **A** in **2**. The N–C(S)S bond (1.263–1.302 Å) is significantly shorter than the N–CH_2 bond (1.464–1.518 Å), which indicates essential double character of the former due to mesomeric effect. Structural features of $[Au(S_2CNR_2)_2]^+$ cations and dithiocarbamate ligands therein were discussed by us in detail previously [19–27].

The counterions of $[Au(S_2CNEt_2)_2]^+$ in the examined complexes are dichloroargentate(I) $[AgCl_2]^-$ (**1**, **2**) and chloride ions (**2**). However, the silver(I)-containing anion in **1** is represented by the 1D polymeric form $([AgCl_2]^-)_n$ (Fig. 3b), while $[AgCl_2]^-$ anions in structure, **2** are discrete (Fig. 4c). In the latter case, the anion has linear structure which is determined by *sp*-hybrid state of the central silver atom (∠ClAgCl 177.02°) with equivalent Ag–Cl bonds (2.3374 Å); the Ag–Cl bond length is very consistent with the sum of covalent (empirical covalent) radii of the silver and chlorine atoms [37]. By contrast, $[AgCl_2]^-$ anions in structure **1** form a polymeric chain, in which the neighboring silver atoms are linked through two

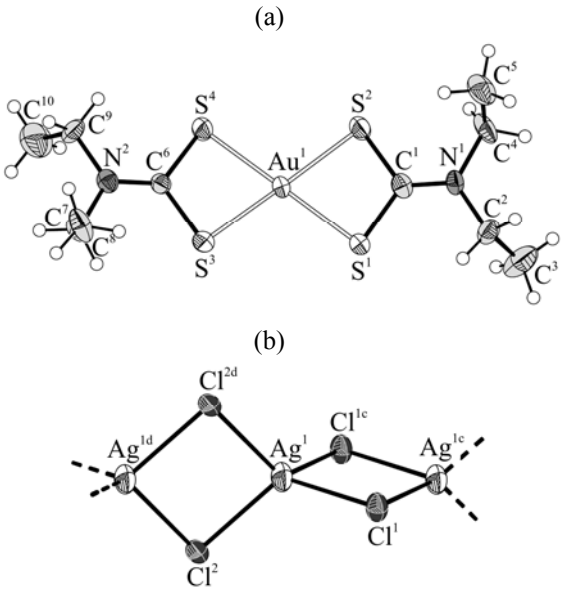

Fig. 3. Structure of the (a) complex anion $[Au(S_2CNEt_2)_2]^+$ and (b) two-unit fragment of the anionic polymeric chain $([AgCl_2]^-)_n$ of complex **1**.

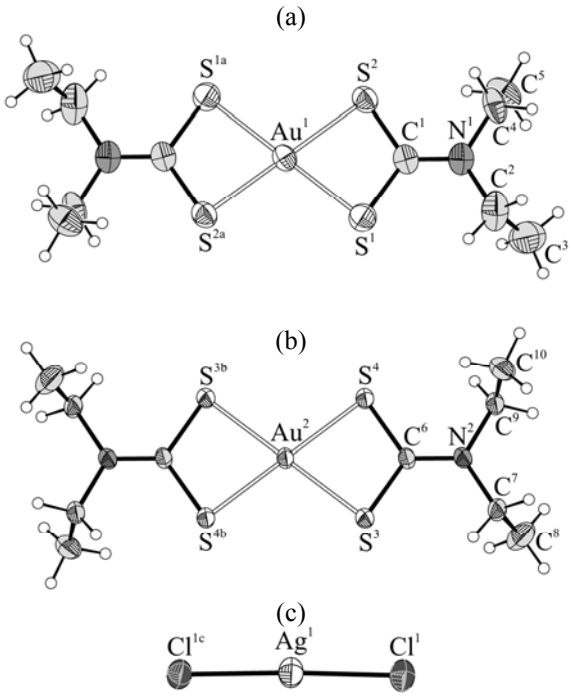

Fig. 4. Structures of (a, b) isomeric complex cations $[Au(S_2CNEt_2)_2]^+$ and (c) discrete anion $[AgCl_2]^-$ of complex **2**.

bridging chlorine atoms (μ_2-bridges, Fig. 3b). The bonds of each chlorine atom with the silver atoms are nonequivalent (Ag–Cl 2.613–2.668 Å; Table 2). However, these bonds seem to be weakened as compared to discrete $[AgCl_2]^-$ anions. On the whole, each silver atoms appears in a distorted tetrahedral environment formed by chlorine atoms (sp^3-hybrid state); the ClAgCl bond angles considerably deviate from the purely tetrahedral value (88.74–123.92°). The AgAgAg angle (175.24°) reflects smooth character of the anionic zigzag chain $([AgCl_2]^-)_n$, where the Ag–Ag interatomic distances are 3.759 and 3.772 Å.

Supramolecular self-organization of both complexes is determined by pair (symmetrical in complex **1** and unsymmetrical in **2**) secondary (non-covalent) Au···S interactions between the cations $[Au(S_2CNEt_2)_2]^+$ (the secondary bonding concept was proposed for the first time to interpret interactions at distances comparable with the sum of the van der Waals radii of the corresponding atoms [38]). Nevertheless, cationic polymeric chains in structures **1** and **2** reveal their radically different supramolecular architectures.

The supramolecular chain formed by complex **1** includes two layers of noncentrosymmetric cations (Fig. 5). Each gold(III) complex cation is linked to the two nearest antiparallel cations of the neighboring layer by two pairs of secondary bonds between the gold atoms and diagonally oriented sulfur atoms S^2 and S^3. The Au^1, Au^{1a}, and Au^{1b} cations are involved in two pairs of symmetric secondary bonds Au^1–S^{2a}, Au^{1a}–S^2 (3.610 Å) and Au^1–S^{3b}, Au^{1b}–S^3 (3.873 Å); the $S^{2a}Au^1S^{3b}$ angle is 52.50°. These interactions give rise to an $\{[Au(S_2CNEt_2)_2]^+\}_n$ zigzag supramolecular chain with the $Au^{1a}Au^1Au^{1b}$ angle 99.06° and interatomic distances Au^1–Au^{1a} 4.683 and Au^1–Au^{1b} 5.198 Å; this chain comprises antiparallel gold(III) cations belonging to two neighboring layers.

Mutual spatial arrangement of the cationic and anionic polymeric chains in structure **1** along the *a* crystallographic axis is shown in Fig. 1. The zigzag cationic chain $([Au\{S_2CN(C_2H_5)_2\}_2]^+)_n$ with two layers of antiparallel cations occupies the central part of a unit cell, and the anionic chains $([AgCl_2]^-)_n$ are located at the corners. The cationic and anionic chains interact with each other via relatively weak but numerous hydrogen bonds C^2–H···Cl^1 and C^9–H···Cl^{2a} (Table 3).

Structural units of complex **2** are isomeric centrosymmetric cations $[Au\{S_2CNEt_2\}_2]^+$, **A** (Au^1) and **B** (Au^2), anions $[AgCl_2]^-$, chloride ions, and hydration water molecules (Figs. 2, 4). The linear supramolecular

Table 2. Selected bond lengths (*d*) and bond angles (ω) and torsion angles (φ) in the complexes $([Au\{S_2CNEt_2\}_2][AgCl_2])_n$ (**1**)[a] and $([Au\{S_2CNEt_2\}_2]_2[AgCl_2]Cl\cdot 2H_2O)_n$ (**2**)[b]

Complex **1**, cation

Bond	*d*, Å	Bond	*d*, Å	Bond	*d*, Å	Bond	*d*, Å
$Au^1–S^1$	2.347(3)	$S^3–C^6$	1.746(14)	$Au^1\cdots S^{2a}$	3.610(4)	$N^1–C^4$	1.475(18)
$Au^1–S^2$	2.333(3)	$S^4–C^6$	1.738(13)	$Au^1\cdots S^{3b}$	3.873(4)	$N^2–C^6$	1.279(16)
$Au^1–S^3$	2.324(4)	$N^1–C^1$	1.263(17)	$S^1–C^1$	1.732(14)	$N^2–C^7$	1.487(18)
$Au^1–S^4$	2.345(3)	$N^1–C^2$	1.498(17)	$S^2–C^1$	1.752(15)	$N^2–C^9$	1.464(17)
Angle	ω, deg	Angle	ω, deg	Angle	ω, deg	Angle	ω, deg
$S^1Au^1S^2$	74.98(13)	$Au^1S^1C^1$	87.6(5)	$S^2Au^1S^3$	172.79(15)	$Au^1S^4C^6$	87.4(5)
$S^1Au^1S^3$	104.34(13)	$Au^1S^2C^1$	87.5(5)	$S^2Au^1S^4$	105.54(13)	$S^1C^1S^2$	109.7(7)
$S^1Au^1S^4$	178.68(11)	$Au^1S^3C^6$	87.9(4)	$S^3Au^1S^4$	74.99(13)	$S^3C^6S^4$	109.3(7)
Angle	φ, deg	Angle	φ, deg	Angle	φ, deg	Angle	φ, deg
$Au^1S^1S^2C^1$	174.6(8)	$S^2C^1N^1C^2$	177.9(9)	$S^3Au^1C^6S^4$	–173.5(7)	$S^4C^6N^2C^7$	–175.3(10)
$Au^1S^3S^4C^6$	–173.0(7)	$S^2C^1N^1C^4$	0.9(18)	$S^1C^1N^1C^2$	–1.5(18)	$S^3C^6N^2C^9$	–178.2(10)
$S^1Au^1C^1S^2$	175.1(7)	$S^3C^6N^2C^7$	3.2(18)	$S^1C^1N^1C^4$	–178.5(11)	$S^4C^6N^2C^9$	3.3(18)

Complex **1**, anion

Bond	*d*, Å	Bond	*d*, Å	Bond	*d*, Å	Bond	*d*, Å
$Ag^1–Cl^1$	2.614(4)	$Ag^1–Cl^{1c}$	2.663(4)	$Ag^1–Cl^2$	2.668(4)	$Ag^1–Cl^{2d}$	2.613(4)
Angle	ω, deg	Angle	ω, deg	Angle	ω, deg	Angle	ω, deg
$Cl^1Ag^1Cl^{1c}$	88.74(11)	$Cl^2Ag^1Cl^{2d}$	89.24(11)	$Cl^1Ag^1Cl^{2d}$	123.92(13)	$Ag^1Cl^1Ag^{1c}$	91.26(11)
$Cl^1Ag^1Cl^2$	120.63(13)	$Cl^{1b}Ag^1Cl^{2d}$	120.17(13)	$Cl^2Ag^1Cl^{1c}$	117.40(13)	$Ag^1Cl^2Ag^{1d}$	90.76(11)

Complex **2**

Cation A		Cation B		Cation A		Cation B	
Bond	*d*, Å	Bond	*d*, Å	Bond	*d*, Å	Bond	*d*, Å
$Au^1–S^1$	2.3216(17)	$Au^2–S^3$	2.3384(12)	$S^2–C^1$	1.709(6)	$S^4–C^6$	1.733(4)
$Au^1–S^2$	2.3280(15)	$Au^2–S^4$	2.3344(12)	$N^1–C^1$	1.288(6)	$N^2–C^6$	1.302(5)
$Au^1\cdots S^{3b}$	3.9569(12)	$Au^2\cdots S^1$	3.7054(16)	$N^1–C^2$	1.518(9)	$N^2–C^7$	1.473(5)
$S^1–C^1$	1.736(5)	$S^3–C^6$	1.730(4)	$N^1–C^4$	1.473(7)	$N^2–C^9$	1.474(5)
Angle	ω, deg	Angle	ω, deg	Angle	ω, deg	Angle	ω, deg
$S^1Au^1S^2$	75.22(6)	$S^3Au^2S^4$	75.43(4)	$Au^1S^2C^1$	87.1(2)	$Au^2S^4C^6$	86.67(15)
$S^1Au^1S^{2a}$	104.78(6)	$S^3Au^2S^{4b}$	104.56(4)	$S^1C^1S^2$	110.9(3)	$S^3C^6S^4$	111.3(2)
$Au^1S^1C^1$	86.7(2)	$Au^2S^3C^6$	86.61(15)				
Angle	φ, deg	Angle	φ, deg	Angle	φ, deg	Angle	φ, deg
$Au^1S^1S^2C^1$	178.8(3)	$Au^2S^3S^4C^6$	179.3(2)	$S^1C^1N^1C^4$	–177.2(4)	$S^4C^6N^2C^7$	–179.0(3)
$S^1Au^1C^1S^2$	178.9(3)	$S^3Au^2C^6S^4$	179.4(2)	$S^2C^1N^1C^2$	175.4(5)	$S^3C^6N^2C^9$	–177.4(3)
$S^1C^1N^1C^2$	–2.9(8)	$S^3C^6N^2C^7$	0.4(6)	$S^2C^1N^1C^4$	1.1(8)	$S^4C^6N^2C^9$	3.2(6)

Anion

Bond	*d*, Å	Angle	ω, deg	Bond	*d*, Å	Angle	ω, deg
$Ag^1–Cl^1$	2.3374(14)	$Cl^1Ag^1Cl^{1c}$	177.02(7)	$Ag^1\cdots S^3$	3.2179(13)	$S^3Ag^1S^{3c}$	137.03(3)

[a] Symmetry transforms: [a] $2-x, 1-y, 1-z$; [b] $1-x, 1-y, 1-z$; [c] $1-x, -y, -z$; [d] $-x, -y, -z$.
[b] Symmetry transforms: [a] $-x, -y, 1-z$; [b] $-x, 1-y, 1-z$; [c] $-x, y, 1/2-z$.

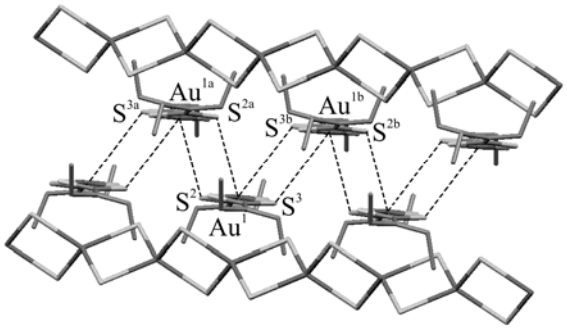

Fig. 5. Zigzag supramolecular cationic chain $([Au\{S_2CNEt_2\}_2]^+)_n$ in the crystal structure of complex **1** (secondary Au···S bonds are shown with dashed lines); anionic polymeric chains $([AgCl_2]^-)_n$ are shown schematically on the top and the bottom (projection onto the *ab* plane).

chains $(\cdots\mathbf{A}\cdots\mathbf{B}\cdots\mathbf{A}\cdots\mathbf{B}\cdots)_n$ (∠AuAuAu 180.00°, $Au^1\cdots Au^2$ 4.069 Å) are formed through secondary interactions involving the gold atoms and diagonal sulfur atoms S^1, S^{1a} and S^3, S^{3b} of isomeric cations; neighboring isomeric cations are linked by pairs of unsymmetrical secondary bonds Au^2–S^1 3.705 Å and Au^1–S^{3b} 3.957 Å (Fig. 6). The chains are oriented along the *b* crystallographic axis, and alternating **A** and **B** cations are arranged in such a way that the bisector axes of the neighboring isomeric cations, passing through both four-membered metallacycles in the bicyclic systems $[CS_2AuS_2C]$, form an angle of 65° while being projected onto the *ac* plane.

In turn, anions $[AgCl_2]^-$ and Cl^- together with outer-sphere water molecules give rise to supramolecular chains $(\cdots[AgCl_2]^-\cdots H–O–H\cdots Cl^-\cdots)_n$ through hydrogen bonds whose parameters are listed in Table 3. The zigzag chains are oriented along the *a* axis between the cationic chains (Fig. 2). In addition, structure **2** features cation-anionic interactions: the silver atoms of linear dichloroargentate(I) ions are involved in paired symmetrical secondary bonds Ag···S

Table 3. Hydrogen bond parameters in the crystal structures of complexes **1**[a] and **2**

Contact D–H···A	Distance, Å			∠DHA, deg
	D–H	H···A	D···A	
C^2–H···Cl^1	0.97	2.76	3.643(15)	152
C^9–H···Cl^{2a}	0.97	2.81	3.670(15)	152
O^{1w}–H^{1wA}···Cl^1	0.88(2)	2.66(3)	3.488(4)	158(5)
O^{1w}–H^{1wB}···Cl^2	0.89(2)	2.38(4)	3.163(4)	148(5)

[a] Symmetry transform: $1-x, -y, 1-z$.

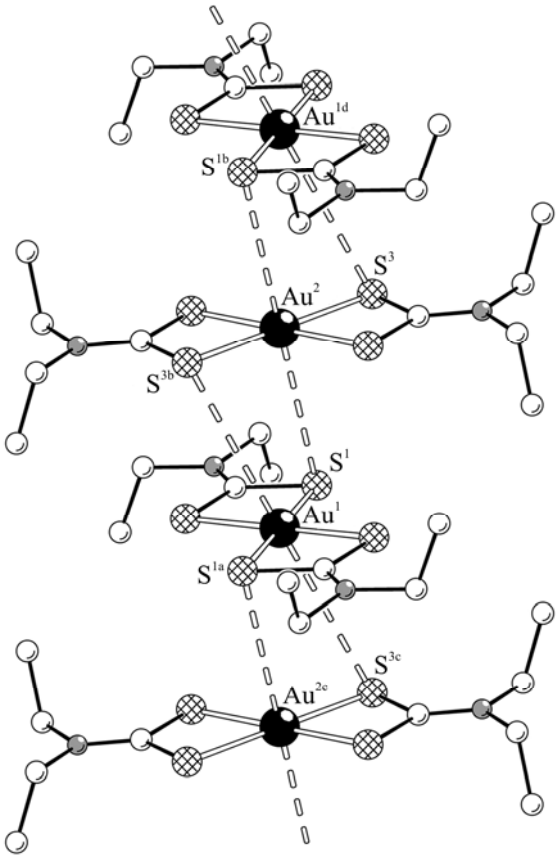

Fig. 6. A fragment of the supramolecular linear cationic chain $(\cdots\mathbf{A}\cdots\mathbf{B}\cdots\mathbf{A}\cdots\mathbf{B}\cdots)_n$ in the crystal structure of complex **2**; secondary Au···S bonds are shown with dashed lines.

(3.2179 Å) with the S^3 atoms of isomeric cations **B**, thus linking two neighboring cationic chains. This provides additional stabilization of structure **2** (for comparison, the sum of the van der Waals radii of the silver and sulfur atoms is 3.52 Å [37]).

The thermal behavior of complexes **1** and **2** was studied in an argon atmosphere using the simultaneous thermal analysis (STA) technique for parallel recording of TG (thermogravimetry) and DSC (differential scanning calorimetry) curves. Despite some differences, the TG curves display similar thermal decomposition patterns of complexes **1** and **2**. Formally, complex **1** decomposes in one step with mass loss of 47.75% (relative to the original one), the main part of which corresponds to the steeply descending section of the TG curve (~145–282°C). Differentiation revealed two inflection point in this region (at 174 and 246°C), which suggests a complicated character of thermal transformations of complex **1**. These transformations involve simultaneously both cation and anion and lead

to the reduction of gold(III) to metal and liberation of AgCl (the calculated value of the residual mass is 50.62%).

The next gently sloping part of the TG curve (from 282 to 835°C, when the residual mass is stabilized) corresponds to final desorption of volatile thermolysis products (8.80%), including thermal dissociation of AgCl. However, the residual mass at 1100°C (43.38%) is somewhat lower than the calculated value (45.34%) for reduced gold and silver. This inconsistency can be explained by the the volatility of the AgCl melt in the high-temperature region. When the thermolysis was complete, light yellow beads were found on the bottom of the crucible without appreciable traces of slag; according to the analytical data, these beads were gold–silver alloy.

The DSC curve showed four endothermic effects. The first low-temperature endotherm is determined by melting of complex **1** with decomposition (extrapolated melting point was estimated at 142.4°C). Independently, by measuring the melting point in a glass capillary we found that complex **1** melts in the temperature range from 140 to 146°C with gas evolution. The two subsequent closely located endotherms having extremes at 236.7 and 255.1°C (extrapolated temperatures 222.6 and 247.6°C) correspond to the maximum mass loss rates at 174–246 and 246–320°C on the TG curve. The high-temperature part of the DSC curve displayed an endotherm due to melting of the reduced metals (extrapolated mp 1031.8°C). According to the phase diagram of the Au–Ag binary metal system, the obtained value is intermediate between the melting points of pure silver and gold (mp 961.78 and 1064.18°C, respectively [39]), and it corresponds to an Au–Ag ratio of 1 : 1 [40] which is consistent with the composition of complex **1**.

The TG curve of complex **2** exhibited several mass loss stages, the first of which was observed in the low-temperature region (~45–115°C); the mass loss was 2.13%, which is close to the calculated value for two outer-sphere hydration water molecules (2.91%). The corresponding endotherm on the DSC curve had extereme at 81.3°C (extrapolated temperature 75.1°C). The next weak endotherm observed at 140.5°C was assigned to melting of the dehydrated complex (extrapolated mp 135.5°C). Independent measurement of the melting point of **2** gave a value in the renge of 136–140.0°C.

A significant mass loss (52.76%) corresponding to the steeply descending part of the TG curve (115–365°C) indicated that the thermolysis process simultaneously involves all complex cations and anions of compound **2** with the reduction of Au(III) to Au(0) and concomitant liberation of AgCl (the calculated and experimental residual weights are 43.42 and 45.11%, respectively). Differentiation of this part of the TG curve revealed two inflection points at 213.0 and 240.0°C, which divide it into three sections, so that the thermal decomposition of **2** is a stepwise process. The DSC curve in this region exhibits two endotherms having extremes at 159.1 and 264.4°C. The final stage (~365–950°C) with a smooth 5.59% weight loss is related to desorption of volatile thermolysis products and reduction of silver in AgCl. The residue at 1100°C was very small Au–Ag alloy beads. Its amount (39.52%), as in the thermolysis of **1**, was somewhat lower than the calculated value for elemental gold and silver (40.56%). In keeping with the presumed formula of **2**, the Au/Ag ratio in the obtained melt was 2 : 1. Therefore, the extrapolated melting point 1046.2°C reflected in the high-temperature region of the DSC curve is considerably higher than the corresponding value for the alloy obtained by thermolysis of **1**. Analysis of the Au–Ag phase diagram also indicated that the extrapolated melting point (1046.2°C) matches the 2 : 1 alloy.

EXPERIMENTAL

The IR spectra were recorded in the range 400–4000 cm^{-1} on a Perkin Elmer Spectrum 65 IR spectrometer with Fourier transform, equipped with attenuated total reflectance accessory. The X-ray diffraction data for single crystals of complexes **1** and **2** were obtained at 296(2) K on a Bruker-Nonius X8 Apex CCD diffractometer (Mo K_α radiation, λ 0.71073 Å, graphite monochromator) according to standard procedure (φ- and ω-scanning of narrow frames). A correction for absorption was applied empirically using SADABS [41]. The structures were solved by the direct method and were refined against F^2 by the least-squares method in full-matrix anisotropic approximation for non-hydrogen atoms. The positions of hydrogen atoms were calculated geometrically and were included in the refinement according to the riding model. Hydrogen atoms of solvate water molecules in structure **2** were localized from the Fourier difference maps, and their positions were refined in isotropic approximation, $U_{iso}(H) = 1.5U_{eq}(O)$. All calculations for structure determination and refinement were performed using SHELXTL software package [41].

The coordinates of atoms, bond lengths, and bond angles were deposited to the Cambridge Crystallographic Data Centre (CCDC entry nos. 1830824 and 1830825 for complexes **1** and **2**, respectively).

The thermal behavior of complexes **1** and **2** was studied by simultaneous thermal analysis (STA) with parallel recording of TG (thermogravimetry) and DSC (differential scanning calorimetry) curves on a Netzsch STA 449C Jupiter instrument. Samples were placed in corundum crucibles capped with holed caps to maintain a pressure of 1 atm during thermal decomposition. Samples were heated at a rate of 5 deg/min to 1100°C in an argon atmosphere; the sample weight was 1.208–4.590 mg; the temperature was measured with an accuracy of ±0.7°C; and the weight change was measured with an accuracy of $\pm 1 \times 10^{-4}$ mg. A correction file was used to record TG and DSC curves, and temperature and sensitivity calibrations were preliminarily performed for the given temperature program and heating rate. The melting points of **1** and **2** were independently measured with a PTP(M) melting point apparatus (*Khimlaborpribor* public corporation).

Initial silver(I) diethyldithiocarbamate was synthesized by reaction of aqueous solutions of silver(I) nitrate and sodium diethyldithiocarbamate trihydrate (Sigma–Aldrich) as described in [3, 42]. According to the ^{13}C and ^{15}N NMR data [42], the complex precipitated from the aqueous phase was polymeric β-modification of $\{[Ag(S_2CNEt_2)][Ag_2(S_2CNEt_2)_2]\}_n$ [3]. IR spectrum, ν, cm^{-1}: 2970, 2935, 2875, 1559, 1482, 1454, 1414, 1375, 1352, 1298, 1263, 1198, 1137, 1093, 1074, 975, 900, 835, 777, 558, 480, 456, 431, 418, 404.

Ion-polymeric bis(diethyldithiocarbamato-*S*,*S*′)-gold(III) dichloroargentate(I), {1, $[Au(S_2CNEt_2)_2][AgCl_2])_n$} and bis(diethyldithiocarbamato-*S*,*S*′) gold(III) chloride dichloroargentate(I) dihydrate {2, $[Au(S_2CNEt_2)_2]_2[AgCl_2]Cl \cdot 2H_2O)_n$} were synthesized by reacting freshly precipitated silver(I) diethyldithiocarbamato with $AuCl_3$ in a 5.15 M solution of sodium chloride (which close to saturation at 20°C). A solution of $Na[AuCl_4]$, 8.0 mL, containing 38.4 mg (0.195 mmol) of gold was added to 100 mg (0.390 mmol) of the silver(I) complex, and the mixture was stirred for 30 min at 60°C. The silver(I) complex successively changed its color from greenish yellow to red–orange and then to white with a yellowish tint and gradually dissolved. The dissolution was complete in 20 min. The products were extracted with chloroform, the extract was concentrated, 2.5 mL of acetone was added to the residue which partially dissolved. From the acetone solution we isolated yellow transparent plates of complex **1**. The mother liquor was dissolved in 3.0 mL of chloroform–acetone (1 : 1), and yellow transparent prisms of complex **2** slowly crystallized therefrom.

$[Au(S_2CNEt_2)_2][AgCl_2]$ (1). IR spectrum, ν, cm^{-1}: 2964, 2927, 2869, 1566, 1457, 1438, 1381, 1353, 1328, 1278, 1188, 1155, 1095, 1076, 1062, 989, 907, 843, 793, 780, 611, 560, 480, 431, 415, 404.

$[Au(S_2CNEt_2)_2]_2[AgCl_2]Cl \cdot 2H_2O$ (2). IR spectrum, ν, cm^{-1}: 3362, 2982, 2937, 2879, 1548, 1459, 1441, 1382, 1351, 1279, 1194, 1154, 1099, 1079, 1063, 990, 907, 847, 781, 609, 560, 520, 483, 464, 431, 417, 410.

The residual amount of gold in solution after extraction was determined by atomic absorption spectroscopy using a Hitachi 180-50 spectrometer. The degree of gold(III) binding by silver(I) diethylcarbamodithioate was 99.95%.

The IR spectra were recorded at the Joint Center, Kurnakov Institute of General and Inorganic Chemistry, Russian Academy of Sciences.

CONFLICT OF INTERESTS

No conflict of interest was declared by the authors.

REFERENCES

1. Hesse, R. and Nilson, L., *Acta Chem. Scand*., 1969, vol. 23, no. 3, p. 825. doi 10.3891/acta.chem.scand.23-0825
2. Jennische, P. and Hesse, R., *Acta Chem. Scand*., 1971, vol. 25, no. 2, p. 423. doi 10.3891/acta.chem.scand.25-0423
3. Anacker-Eickhoff, H., Hesse, R., Jennische, P., and Wahlberg, A., *Acta Chem. Scand., Ser. A*, 1982, vol. 36, no. 3, p. 251. doi 10.3891/acta.chem.scand.36a-0251
4. Zhang, W.G., Zhong, Y., Tan, M.Y., Liu, W.S., and Su, C.Y., *Chin. J. Chem*., 2002, vol. 20, no. 5, p. 420. doi 10.1002/cjoc. 20020200503
5. Liu, N., Fan, J., Zhang, W.-G., Yin, X., and Xie, M.-B., *Acta Crystallogr., Sect. E*, 2006, vol. 62, no. 7, p. m2588. doi 10.1107/S1600536806032314
6. Song, Y.-W., Yu, Z., and Zhang, Q.-F., *Acta Crystallogr., Sect. C*, 2006, vol. 62, no. 5, p. m214. doi 10.1107/S0108270106006688
7. Yin, X., Xie, M.-B., Zhang, W.-G., and Fan, J., *Acta Crystallogr., Sect. E*, 2007, vol. 63, no. 9, p. m2273. doi 10.1107/S1600536807035180

8. Ehsan, M.A., Khaledi, H., Tahir, A.A., Ming, H.N., Wijayantha, K.G.U., and Mazhar, M., *Thin Solid Films*, 2013, vol. 536, p. 124. doi 10.1016/j.tsf.2013.03.092
9. Mothes, R., Petzold, H., Jakob, A., Rüffer, T., and Lang, H., *Inorg. Chim. Acta*, 2015, vol. 429, p. 227. doi 10.1016/j.ica.2015.02.008
10. Mothes, R., Jakob, A., Waechtler, T., Schulz, S.E., Gessner, T., and Lang, H., *Eur. J. Inorg. Chem*., 2015, vol. 2015, no. 10, p. 1726. doi 10.1002/ejic.201403182
11. Banti, C.N. and Hadjikakou, S.K., *Metallomics*, 2013, vol. 5, no. 6, p. 569. doi 10.1039/c3mt00046j
12. de Paiva, R.E.F., Abbehausen, C., Gomes, A.F., Gozzo, F.C., Lustri, W.R., Formiga, A.L.B., and Corbi, P.P., *Polyhedron*, 2012, vol. 36, no. 1, p. 112. doi 10.1016/j.poly.2012.02.002
13. Azócar, M.I., Gómez, G., Velásquez, C., Abarca, R., Kogan, M.J., and Páez, M., *Mater. Sci. Eng., C*, 2014, vol. 37, p. 356. doi 10.1016/j.msec.2014.01.033
14. Aslanidis, P., Hatzidimitriou, A.G., Andreadou, E.G., Pantazaki, A.A., and Voulgarakis, N., *Mater. Sci. Eng., C*, 2015, vol. 50, p. 187. doi 10.1016/j.msec.2015.02.014
15. Ronconi, L., Giovagnini, L., Marzano, C., Bettío, F., Graziani, R., Pilloni, G., and Fregona, D., *Inorg. Chem*., 2005, vol. 44, no. 6, p. 1867. doi 10.1021/ic048260v
16. Keter, F.K., Guzei, I.A., Nell, M., van Zyl, W.E., and Darkwa, J., *Inorg. Chem*., 2014, vol. 53, no. 4, p. 2058. doi 10.1021/ic4025926
17. Boscutti, G., Feltrin, L., Lorenzon, D., Sitran, S., Aldinucci, D., Ronconi, L., and Fregona, D., *Inorg. Chim. Acta*, 2012, vol. 393, p. 304. doi 10.1016/j.ica.2012.06.048
18. Shi, Y., Chu, W., Wang, Y., Wang, S., Du, J., Zhang, J., Li, S., Zhou, G., Qin, X., and Zhang. C., *Inorg. Chem. Commun*., 2013, vol. 30, p. 178. doi 10.1016/j.inoche.2013.02.010
19. Rodina, T.A., Ivanov, A.V., Loseva, O.V., Zaeva, A.S., and Gerasimenko, A.V., *Russ. J. Inorg. Chem*., 2013, vol. 58, no. 3, p. 338. doi 10.1134/S0036023613030133
20. Rodina, T.A., Ivanov, A.V., and Gerasimenko, A.V., *Russ. J. Coord. Chem*., 2014, vol. 40, no. 2, p. 100. doi 10.1134/S1070328414020080
21. Ivanov, A.V., Loseva, O.V., Rodina, T.A., Gerasimenko, A.V., and Sergienko, V.I., *Dokl. Phys. Chem*., 2013, vol. 452, no. 2, p. 223. doi 10.1134/S0012501613100011
22. Zaeva, A.S., Ivanov, A.V., Gerasimenko, A.V., and Sergienko, V.I., *Russ. J. Inorg. Chem*., 2015, vol. 60, no. 2, p. 203. doi 10.1134/S0036023615020229
23. Loseva, O.V., Rodina, T.A., Gerasimenko, A.V., and Ivanov, A.V., *Russ. J. Coord. Chem*., 2017, vol. 43, no. 5, p. 286. doi 10.1134/S1070328417050049
24. Rodina, T.A., Loseva, O.V., Smolentsev, A.I., and Ivanov, A.V., *J. Struct. Chem*., 2016, vol. 57, no. 1, p. 146. doi 10.1134/S0022476616010182
25. Rodina, T.A., Loseva, O.V., Gerasimenko, A.V., and Ivanov, A.V., *Russ. J. Inorg. Chem*., 2013, vol. 58, no. 9, p. 1104. doi 10.1134/S0036023613090179
26. Loseva, O.V., Rodina, T.A., Smolentsev, A.I., and Ivanov, A.V., *Polyhedron*, 2017, vol. 134, p 238. doi 10.1016/j.poly.2017. 06.021
27. Ivanov, A.V., Bredyuk, O.A., Loseva, O.V., and Antsutkin, O.N., *Russ. J. Inorg. Chem*., 2016, vol. 61, no. 6, p. 755. doi 10.1134/S0036023616060103
28. Exarchos, G., Robinson, S.D., and Steed, J.W., *Polyhedron*, 2001, vol. 20, nos. 24–25, p. 2951. doi 10.1016.S0277-5387(01)00885-3
29. Bellamy, L.J., *The Infra-red Spectra of Complex Molecules*, London: Methuen, 1958.
30. Byr'ko, V.M., *Ditiocarbamaty* (Dithiocarbamates), Moscow: Nauka, 1984.
31. Fabretti, A.C., Forghieri, F., Giusti, A., Preti, C., and Tosi, G., *Spectrochim. Acta, Part A*, 1984, vol. 40, no. 4, p. 343. doi 10.1016/0584-8539(84)80059-8
32. Odola, A.J. and Woods, J.A.O., *J. Chem. Pharm. Res*., 2011, vol. 3, no. 6, p. 865.
33. Yin, H., Li, F., and Wang, D., *J. Coord. Chem*., 2007, vol. 60, no. 11, p. 1133. doi 10.1080/00958970601008846
34. Khitrich, N.V. and Seifullina, I.I., *Russ. J. Coord. Chem*., 2000, vol. 26, no. 11, p. 798.
35. Nakamoto, K., *Infra-Red Spectra of Inorganic and Coordination Compounds*, New York: Wiley, 1963.
36. Langaro, A.P., Souza, A.K.R., Morassuti, C.Y., Lima, S.M., Casagrande, G.A., Deflon, V.M., Nunes, L.A.O., and Andrade, L.H.C., *J. Phys. Chem. A*, 2016, vol. 120, no. 46, p. 9249. doi 10.1021/asc.jpca.6b08158
37. Winter, M., WebElements. The Periodic Table of the Elements. http://www.webelements.com. Accessed January 2010.
38. Alcock, N.W., *Adv. Inorg. Chem. Radiochem*., 1972, vol. 15, no. 1, p. 1. doi 10.1016/S0065-2792(08)60016-3
39. Lidin, R.A., Andreeva, L.L., and Molochko, V.A., *Konstanty neorganicheskikh veshchestv: spravochnik* (Constants of Inorganic Compounds. Reference Book), Moscow: Drofa, 2008.
40. *Diagrammy sostoyaniya dvoinykh metallicheskikh sistem: spravochnik* (Phase Diagrams of Binary Metallic Systems), Lyakishev, N.P., Ed., Moscow: Mashinostroenie, 1996.
41. APEX2 (Version 1.08), SAINT (Version 7.03), SADABS (Version 2.11), and SHELXTL (Version 6.12), Madison, WI, USA: Bruker AXS, 2004.
42. Ivanov, A.V., Zinkin, S.A., Konzelko, A.A., and Forsling, W., *Russ. J. Inorg. Chem*., 2004, vol. 49, no. 4, p. 593.